Icarus 421 (2024) 116242

Contents lists available at ScienceDirect

Icarus

journal homepage: www.elsevier.com/locate/icarus

Wintertime column modeling in Jezero crater, Mars: Period of near-fog and a dust event

Hannu Savijärvi [a,b,*], Jouni Polkko [b], Maria Hieta [b], German Martinez [c], Maria-Paz Zorzano [d], Leslie Tamppari [e], Joonas Leino [b], Mark Paton [b], Ari-Matti Harri [b]

[a] Institute for Atmospheric and Earth System Research, University of Helsinki, Finland
[b] Finnish Meteorological Institute, Helsinki, Finland
[c] Lunar and Planetary Institute, Houston, TX, USA
[d] Centro de Astrobiologia, CSIC-INTA, Madrid, Spain
[e] Jet Propulsion Laboratory/California Institute of Technology, Pasadena, CA, USA

ARTICLE INFO

Keywords:
Mars, climate
Mars, surface
Meteorology

ABSTRACT

The diurnal water cycle was studied at a Jezero crater base site using M2020 observations and adsorptive column modeling in a cool midwinter period just before a dust peak and at the peak. During low-dust sols 566–571 the observed air relative humidity (RH) at 1.45 m height was high, 40–90% near dawn. For the typical nocturnal wind speed of 2 m/s at 1.45 m and column water of 9.7 μm, the model's diurnal air temperatures and RH were within observations. For weaker winds model-RH increased as in some of the observed sols. In a nearly calm experiment fog formed from 1.45 m upward. Ground frost appeared independently of wind, but only if adsorption was disabled. The dust peak at around sol 577 was also well simulated with the same wind and absolute humidity as before the event, but relative humidities dropped dramatically due to the dust-enhanced higher nocturnal temperatures.

1. Introduction

The Mars 2020 (M2020) mission rover "Perseverance" landed onto the Jezero crater, Mars (18.44°N, 77.45°E) in February 2021 at the beginning of the local northern hemisphere spring of Martian year 36. The rover carries the Mars Environmental Dynamics Analyzer (MEDA, Rodriguez-Manfredi et al., 2021). MEDA measures, among other quantities, ground surface temperature T_g via a remote thermal infrared sensor (TIRS, Martinez et al., 2023) and air surface pressure P via a pressure sensor (PS, Sánchez-Lavega et al., 2023, Harri et al., 2024). Three air temperature sensors (ATS, Munguira et al., 2023), a wind sensor (WS, Newman et al., 2022, Viúdez-Moreiras et al., 2022) and a humidity sensor (HS) are located at 1.45 m height in a mast to minimize thermal influence from the rover. The humidity instrument and initial results from it interpreted by some column modeling have been described in Hieta et al. (2022) and Polkko et al. (2023).

Fogs and frost have not been detected during the first Perseverance year of 669 sols on Mars, although the MEDA-derived daily near-dawn maximum relative humidity at the 1.45 m height (max RH) occasionally exceeded 100% in the cold midwinter period of MY36 (Fig. 1a,b). On sols 565–591 the rover stayed parked in the Jezero delta front area (Fig. 2). We study MEDA data at this sample-collecting site ("Shuyak" in Zorzano et al., 2024) during the low dust high-RH sols just before the arrival of a local dust event (Fig. 1c), and then at around the dust peak. Moderate dust-transporting wind and wind-assisted (i.e., forced) daytime convection is thus likely during these periods.

During sols 566–571 (Ls 308°-312°) the observed 880 nm dust opacity τ was still low, about 0.5, but the daily max RH (relative to ATS temperature) was quite high, with occasional values >100% near the dawn of sol 566. However, fog and frost were not detected although specific campaigns to detect them were not launched for this period. Unfortunately, wind observations are not available, the wind sensor being damaged during a regional dust storm around sol 312. We hence perform here experiments, by varying wind speeds in the University of Helsinki/Finnish Meteorological Institute single-column model (SCM), in order to analyze the near-surface temperatures and moistures, and to assess whether fogs, frost and boundary layer ice clouds would have been expected, if winds had been weak enough. The wind-enhanced surface flux of moisture (with diffusion and adsorption of water vapor in the soil pores) plays here a large role, near-calm conditions being

* Corresponding author at: INAR/Physics, Faculty of Science, 00014, University of Helsinki, Finland.
E-mail address: hannu.savijarvi@helsinki.fi (H. Savijärvi).

https://doi.org/10.1016/j.icarus.2024.116242
Received 13 June 2024; Received in revised form 13 July 2024; Accepted 31 July 2024
Available online 2 August 2024

favorable for free convection at daytime and very weak turbulence at night.

We then consider the dust peak sols 576–578, when τ had rapidly increased from 0.5 up to ~1.8, thereafter declining slowly. The arriving windy airmass was hence quite dusty, whereas the observed max RH dropped dramatically (Fig. 1). Whether the dusty airmass was hence also much drier than the one it replaced is discussed displaying MEDA observations and model simulations during the dust peak period. Our conclusions are given in the end.

2. Model experiments

The MEDA HS-measured air-RH = $p/p_{sat}(T)$ (p being the water vapor partial pressure and p_{sat} the saturation water vapor pressure over ice), and the derived water vapor volume mixing ratio vmr = p/P (where P is the total atmospheric pressure measured by MEDA PS) are quite sensitive to the ambient air temperature T (measured by MEDA ATS), due to the strong Clausius-Clapeyron dependence of p_{sat} on temperature (Polkko et al., 2023). Hence the modeled ambient air temperatures at 1.45 m should be quite accurate for any meaningful comparison between the modeled and the HS-ATS -P -based (observed) air moisture variables RH and vmr.

Our experiments are made using the UH/FMI hydrostatic atmosphere-regolith single-column model, SCM (without advection and vertical motion), which is here forced by constant geostrophic wind speed Vg. There are 29 air points, from 0.3, 0.7, 1.45, 3.5, 8.0 m … to 40 km, and eight grid points in the ground. The model's physical parameterizations produce among other things the turbulent surface fluxes for momentum, heat and humidity, and the solar and thermal radiation. These drive thermal diffusion in the ground and molecular diffusion of moisture in the air pores of porous regolith. Parameterizations of moisture also include possible condensation and sublimation of frost, ice fog and boundary layer ice clouds (as in Savijärvi and Määttänen (2010) for Phoenix), and adsorption and desorption of water vapor in porous regolith (Savijärvi et al., 2016, 2020). For adsorption, which is enhanced

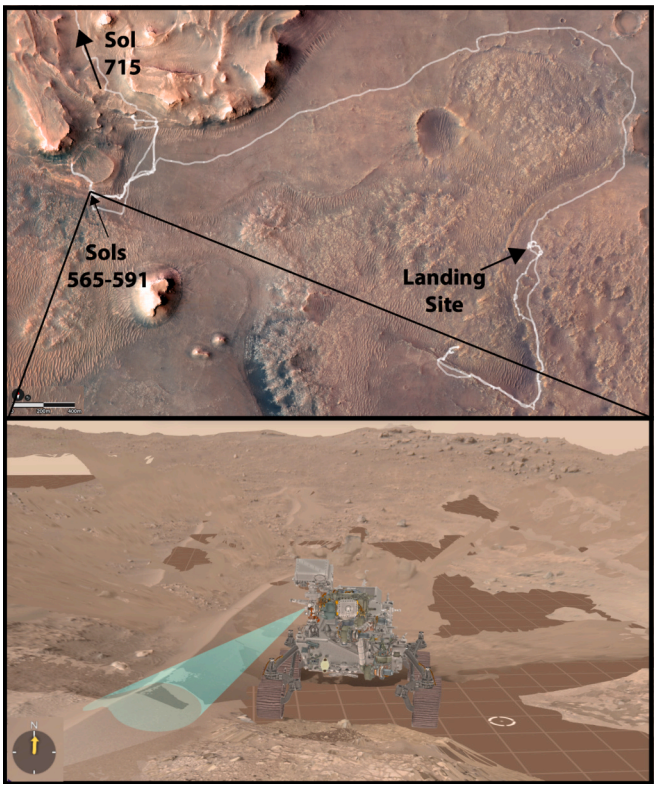

Fig. 2. The M2020 Perseverance rover route in the Jezero crater, its stationary location during sols 565–591 and the scenery at this site showing the TIRS downscan field of view (FoV) at the surface. Ground thermal inertia for this 3–4 m^2 spot is ~280 SI units and noon surface albedo ~0.15, estimated via the methods of Martínez et al. (2023) and using dust-cover corrected solar flux observations.

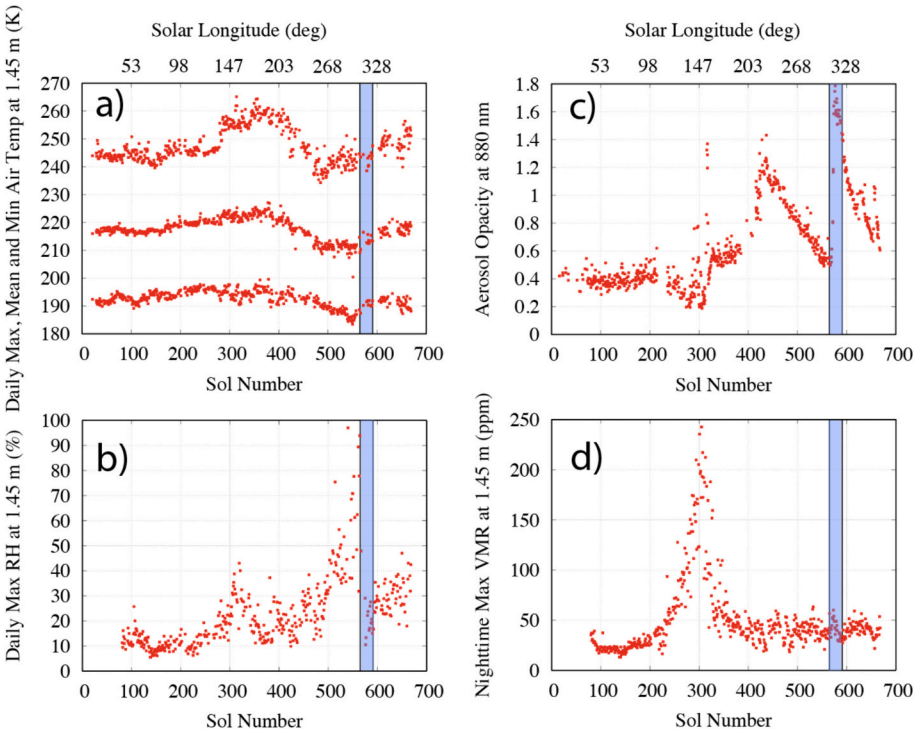

Fig. 1. The daily (a) maximum, minimum and mean air temperatures, (b) maximum relative humidities at sensor board temperature, (c) dust opacities, and (d) the nighttime maximum vmr during the first M2020 year, with sols 565–591 marked. The numbers at the top (solar longitude Ls) indicate seasons at Jezero, Ls 90° (270°) being the northern summer (winter) solstice.

by low T and high vmr (obeying the Clausius-Clapeyron -like van't Hoff equilibrium equation, Savijärvi and Harri, 2021), the Jakosky et al. (1997) adsorption isotherm is adopted. Model validations have been provided for air temperatures using MER mini-TES soundings in Savijärv (2012), for surface fluxes using MEDA observations in Martínez et al. (2023), and for MEDA air moistures in Polkko et al. (2023).

Local turbulence is handled in the SCM via a wind speed-, roughness- and stability-dependent Monin-Obukhov scheme for the lowest air layer and via a mixing length approach aloft. The adopted stability function (Ri being the bulk Richardson number of any air layer) is $f(Ri) = (1 + 5Ri + 25Ri^2)^{-1}$ for stable layers (Zilitinkevich et al. (2002), using Ri_{crit} of 0.20). This *Z*-function fits the standard Dyer-Businger (DB) form (e.g. Garratt, 1992) in windy weakly stable conditions but allows for super-critical stratification ($Ri > Ri_{crit}$), having been validated by very stable Antarctic (Halley observatory) data. For unstable layers ($Ri < 0$) the Grachev et al. (2000) G-functions ($f_m(Ri) = (1\text{-}10Ri)^{0.333}$ for momentum; $f_h(Ri) = (1\text{-}34Ri)^{0.333}$ for heat and humidity) are adopted, as they fit the DB functions during near-neutral windy conditions but approach (unlike DB) the energetically correct free convection limit for very weak winds, which are included in our test cases. The values of these stability functions are compared in Table 1.

Model experiments are made by fixing Ls, the (constant) dust visible optical depth τ and the mean surface pressure P from M2020 observations, setting the geostrophic wind Vg and roughness length z_o to typical values (10 m/s, 1 cm) and varying the ground thermal inertia and surface albedo, until the model's air temperatures T at 1.45 m match the ATS observations. After this, the value for the initially vertically constant (= well-mixed) vmr is varied with porosity (air fraction of the ground) fixed to a typical value of 30%, until the model's diurnal vmr at 1.45 m is within the observation-derived vmr. Finally, porosity is varied until the model's diurnal vmr remains within the available observations from sol to sol (i.e. without rapid unphysical growth or decay). Hence the model's column precipitable water content (pwc, integral of vmr over pressure) is approximately conserved in the time scale of a few sols.

Then Vg is varied, keeping the other input parameters unchanged, to find out the effects on the behavior of temperatures, moistures, fogs, frosts and the surface fluxes. Experiments are also made by excluding adsorption and/or diffusion of moisture within the soil. The results shown are from the model's sol 3, when it keeps repeating its diurnal cycles for winds, temperatures and moistures from sol to sol.

3. The windy reference simulation for sols of high relative humidity

Perseverance was stationary during sols 566–571 (Ls 308°-312°), the observed dust optical depth τ being low, about 0.5. The derived maximum daily values of relative humidity were quite high during this period, whereas values of vmr were relatively low and stable (Fig. 1). The model is initialized here for Ls of 310°, τ of 0.5 and P of 740 Pa. Then, for ground thermal inertia of 300 SI units, noon albedo of 0.17, porosity of ground 0.22, initial vmr of 120 ppm and Vg of 10 m/s (the reference simulation) the model produces a repeating diurnal cycle of temperatures and vmr, which at the 1.45 m height are within the MEDA observations of the period (Fig. 3), except for a cold morning bias to be explained later. The observed T and vmr display small rapid random-like and correlated fluctuations at night in Fig. 3, suggesting windshear-driven nocturnal turbulence near the surface (Pla-García et al., 2023). The T-fluctuations are larger at daytime, suggesting strong turbulence by convection (Munguira et al., 2023).

Table 1
Values of stability functions DB, Z and G as function of Richardson number Ri.

Ri	$f_{m,h}$	$f_{m.h}$	Ri	f_m	f_m	f_h	f_h
Stable:	DB	Z	Unstable:	DB	G	DB	G
0.05	0.75	0.76	−0.1	1.26	1.26	1.58	1.59
0.1	0.50	0.57	−0.5	1.71	1.82	2.92	3.30
0.2	0	0.33	−1	2.00	2.22	4.00	4.94
0.3	–	0.21	−2	2.36	2.76	5.56	7.61

In this "windy" reference simulation (Vg 10 m/s) the modeled wind speed at 1.45 m height is ~6 m/s around midday, as typically measured by the MEDA wind sensor earlier in the mission, when the device was operating nominally (Newman et al., 2022). During the night the model's wind speed of ~2 m/s is at the top of the typical WS-observed range (0.1–2 m/s). Model-pwc stays here at around 9.7 μm from sol to sol, close to the orbit-observed values (~10 μm) from CRISM and TES over Jezero during this season (Pla-García et al., 2020).

The model's midafternoon vmr at 1.45 m is ~127 ppm in the windy reference simulation (black dashed curves in Fig. 3, top), but is then strongly depleted mainly by adsorption during the late afternoon and evening, owing to wind-shear driven turbulence mixing water molecules toward the ground to become adsorbed to the coooling top regolith. The resulting nocturnal surface inversion of moisture extends to about 250 m height. Desorption and strong convection then mix the adsorbed moisture back to the air during the warm midday hours. Water vapor is hence evenly mixed to about 120 ppm throughout the growing convective boundary layer (CBL); up to 5 km height in the afternoon. The weak wind simulations are discussed in detail in the next section.

Fig. 4 shows the TIRS-measured ground surface temperature T_g at the 3–4 m^2 field of view (FoV, Fig. 2), together with model-T_g. The latter represents "areal" T_g for the footprint area, over which winds bring air to the air sensors (Savijärvi et al., 2023). The observed and modeled T_g are here nearly the same at night during sols 566–569 when both the observed and model-τ were 0.5. The observed afternoon-T_g is slightly higher than model's, in accordance with the slightly lower thermal inertia (280 vs. 300) and albedo (0.15 vs. 0.17) derived for the regolith-dominated small TIRS FoV (Fig. 2). The observed values of T_g and air-T are getting lower in the afternoons and higher at nights during sols 570 and 571 (violet and brown dots in Figs. 3 and 4), as τ is already increasing (0.61 at sol 570 and 0.80 on sol 572) due to the approaching dust event.

The model-T_g is clearly too cool soon after sunrise in Fig. 4, due to our use of a constant areal-TI. Such cold morning bias in model-T_g, and hence in model's air-T as well (c.f. Fig. 3) suggests that the apparent areal thermal inertia of the ground is not temporally constant. It is probably quite low just after sunrise, due to inhomogeneities in the soil (Savijärvi et al., 2022; Savijärvi et al., 2023; Martínez et al., 2023).

The model-T_g is nearly independent of wind speed in Fig. 4, as T_g is strongly driven by the radiation balance in Mars (Petrosyan et al., 2011; Martínez et al., 2023). Model's air temperature is instead more sensitive to the wind speed in Fig. 3. This will be commented in Section 6.

4. Experiments with weaker winds

As winds were not observed but relative humidities were close to and even perhaps above 100% during sols 566–571, it is interesting to assess whether weak winds could be associated with the high measured values of RH. Fig. 5 presents a close look of the MEDA HS-ATS -derived air relative humidities at 1.45 m height. They rise rapidly from sunset onward with large sol-to-sol and within-sol scatter, ending up to 40%–90% RH near sunrise, then decreasing very rapidly. Some individual values from sol 566 (blue dots) even exceed 100% RH in the ambient air, indicating supersaturation and possibly fog. However, fog observations are not reported during this or any other period during MY36.

Fig. 5 also displays hourly RH at 1.45 m from three SCM simulations. The lowest curve (black) amid the late-night observations, is from the windy reference simulation (V_g 10 m/s), where winds at the 1.45 m height are ~2 m/s during the night. Its RH reaches to 73% by dawn. The middle curve is from a simulation with Vg of 2 m/s. Here the wind at 1.45 m is weak, ~ 0.75 m/s during the night. This reduces the windshear-driven nocturnal turbulence and hence adsorption, with vmr staying at a higher level at night than in the windy simulation (Fig. 3,

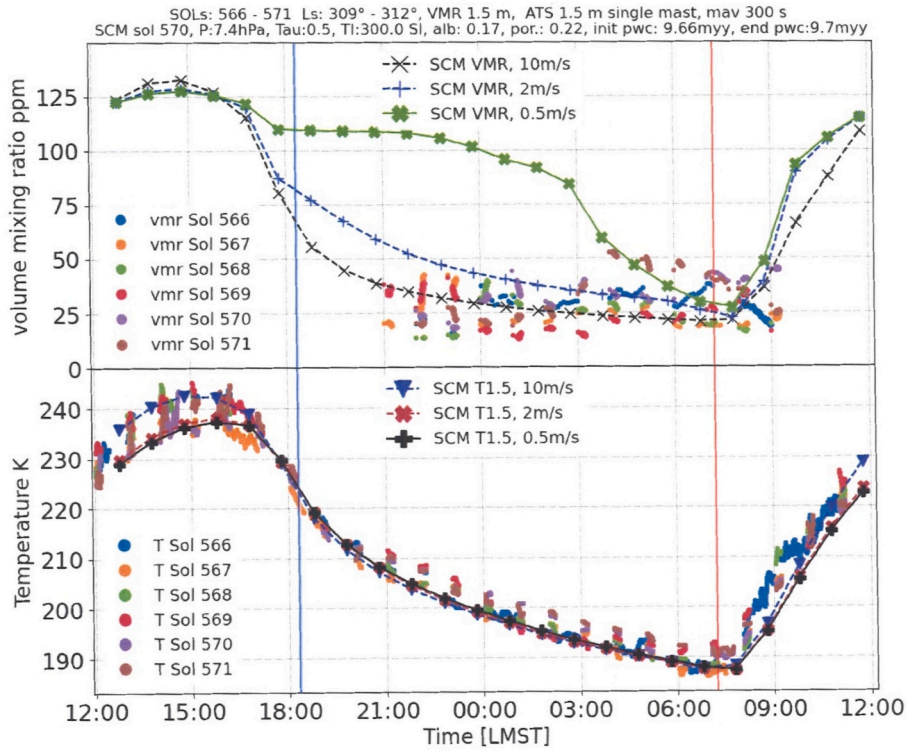

Fig. 3. Water vapor volume mixing ratios (vmr) at 1.45 m height derived from MEDA observations of HS, PS and ATS for sols 566–571 (top), and the respective ATS single-mast air temperatures at 1.45 m (bottom; 300 s moving average) in Mars hours local mean solar time (LMST). Curves are vmr and T at 1.45 m height from SCM simulations ($\tau = 0.5$) for geostrophic wind speeds of 10 m/s (windy), 2 m/s (weak wind) and 0.5 m/s (nearly calm). Blue and red vertical lines indicate sunset and sunrise, respectively. There is fog at 0400–0700 in the nearly calm simulation (= green vmr). (For interpretation of the references to colour in this figure legend, the reader is referred to the web version of this article.)

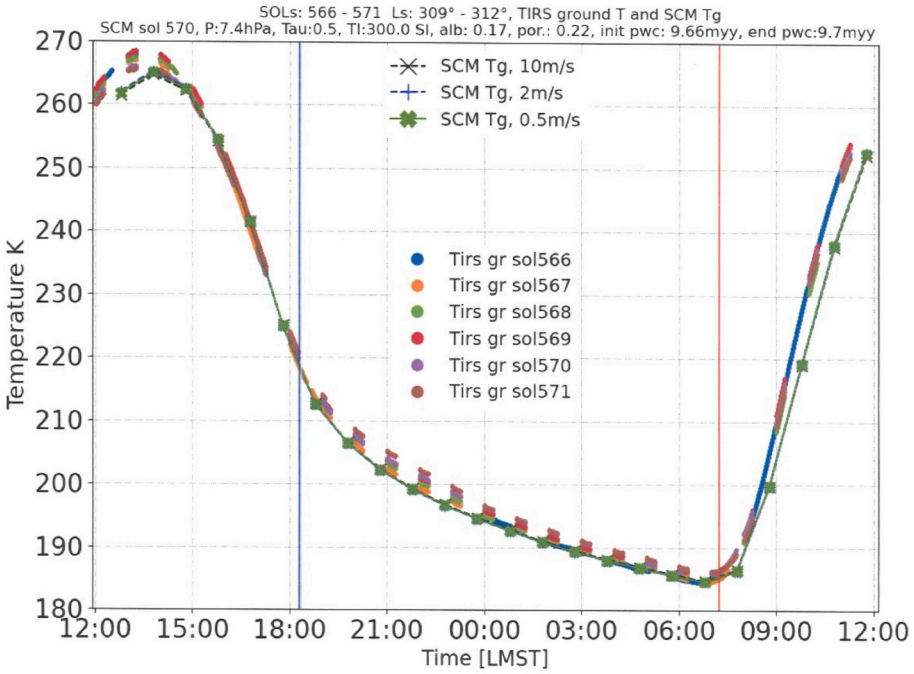

Fig. 4. MEDA TIRS-FoV (Fig. 2) ground surface temperatures T_g (Tirs gr) for sols 566–571, and T_g from the three SCM simulations of Fig. 2 (three overlapping lines).

top). Air-RH hence gets higher at night. It is now at the top range of the late-night observations and reaches 91% at dawn.

The top curve in Fig. 5 is for Vg of 0.5 m/s. The wind speed at 1.45 m height is here only ~0.44 m/s during day and night. Nocturnal stability is now in the supercritical range, shear-driven turbulence is suppressed and adsorption is strongly inhibited as the downward flux of moisture is negligible (Section 6). Hence vmr decreases only slowly in the evening (Fig. 3, top). The near-surface RH now increases rapidly after sunset and

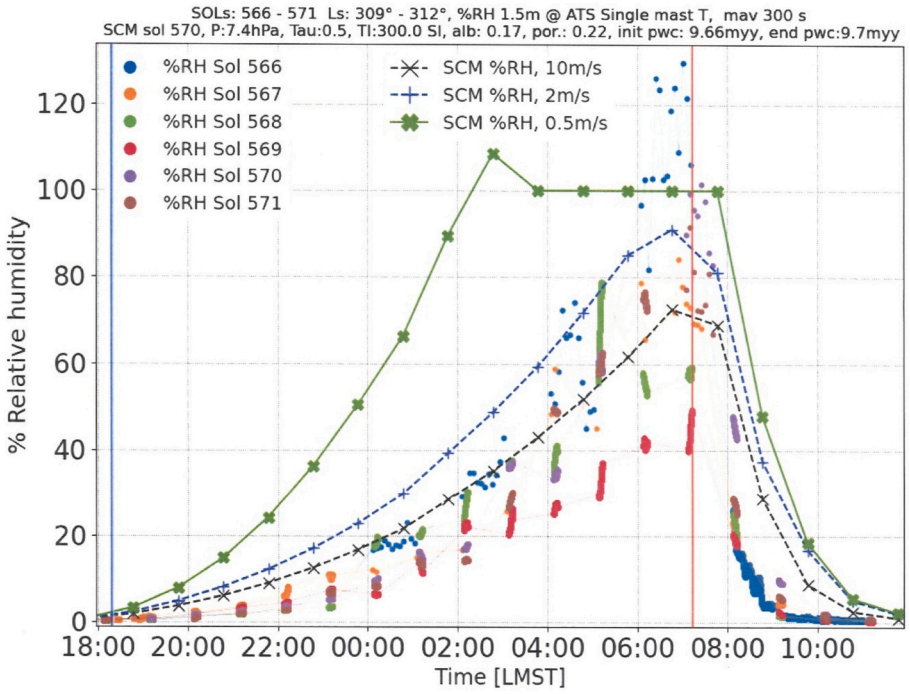

Fig. 5. MEDA-derived relative humidities at ATS temperatures for sols 566–571, and RH at 1.45 m height from the three SCM simulations of Figs. 3–4. The nearly calm simulation leads here to thin fog (100% RH) at 0400- ~ 0800 LMST, but not to frost. Sol 566 (blue dots) may have been less windy near the dawn, and sol 569 (red dots) windier than the other sols. (For interpretation of the references to colour in this figure legend, the reader is referred to the web version of this article.)

reaches 109% at 0200 LTST (0240 LMST). In the model, ice is assumed to condense onto dust particles at a slight supersaturation (RH of 120%, Savijärvi and Määttänen, 2010), after which condensation (i.e. freezing) can take place at 100% RH onto the now ice-covered dust particles. A thin typical calm-air radiation fog appears as a result at about 0300 LMST at the 1.45 m height. It grows from 1.45 m up to 40 m by dawn but disappears (sublimates) soon after sunrise. Frost is not formed. The fog is very thin (its maximum precipitable ice content is only 0.03 μm at dawn), but the experiment suggests that radiation fogs might be detectable as blurred camera pictures just around and after dawn, and possibly as reduced (increased) values in the downwelling shortwave (longwave) radiation, compared to the same-time observations from nearby sols without fog.

Fig. 3 (top) presented the observed and simulated nocturnal values of air-vmr. The windy simulation is in the midst of the observation-based values and the Vg 2 m/s simulation is near the upper limit of them before 0300 LMST. However, after 0300 LMST both the observed vmr and RH tend to display high values during many sols in Figs. 3 and 5. This might indicate that winds then became temporarily weak at this site. Winds are perhaps particularly weak near the dawn of sol 566, when the observation-based vmr displays a sudden increase (blue dots in Fig. 3), and the observed RH simultaneously exceeds 100% (blue dots in Fig. 5). On the other hand, the late night on sol 569 may have been quite windy as its observed vmr and RH (red dots in Figs. 3 and 5) are low.

In the nearly calm simulation (Vg 0.5 m/s, green in Fig. 3) vmr displays only a little depletion during the evening, as adsorption is strongly inhibited by lack of turbulence. From about 0300 LMST onward condensation to fog phase (Fig. 5) depletes the amount of vapor phase (i.e., vmr) at the 1.45 m height quite strongly.

5. Excluding adsorption and diffusion of moisture in the simulations

We also made two hypothetical windy-case (V_g 10 m/s) simulations. In the first adsorption and desorption were disabled but molecular diffusion of water vapor through pore-CO_2 was allowed. Here the vmr at 1.45 m height declines only slowly, from ~120 ppm at midday to about 100 ppm in the evening (Fig. 6, top, ads = 0), as molecular diffusion is a relatively weak process and adsorption was excluded. Air-RH hence rises rapidly during the moist evening, despite the wind, until the frost point is reached at the cold ground. Frost then starts to deposit strongly on the ground from about 2300 local true solar time (LTST) onward, depleting

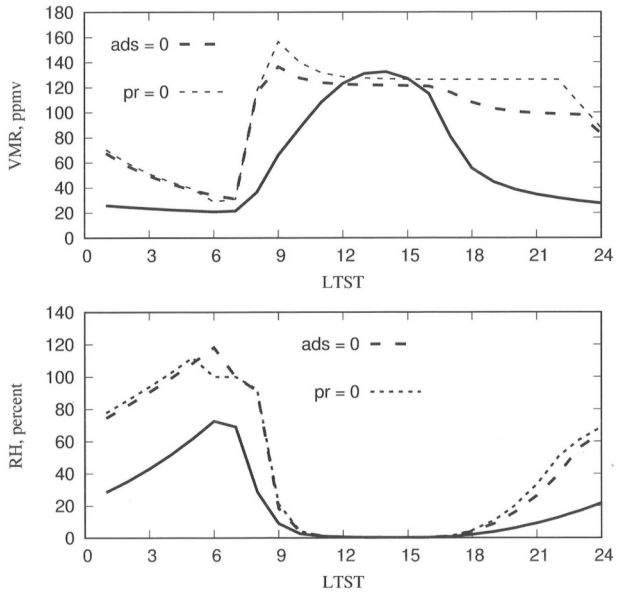

Fig. 6. VMR and RH at 1.45 m height in Mars hours local true solar time (LTST) from the windy SCM simulation (solid lines); the same but with adsorption excluded (ads = 0; dashed lines), and the same but porosity set to 0 (pr = 0; dotted lines). Frost deposits at the surface from 2200 when pr = 0, and from 2300 when ads = 0 (depleting the near-air vmr), with thin fog (RH 100%) appearing near sunrise in both. Fog and frost sublimate away during 0700–0900, temporarily increasing air-vmr at 1.45 m.

the near-surface air-vmr down to 35 ppm by sunrise. Furthermore, thin fog appears here at 1.45 m just around sunrise.

In the second hypothetical Vg 10 m/s simulation with unchanged TI and albedo, ground porosity is set to 0 (as for bedrock). This cuts off both diffusion and adsorption. Model-vmr at 1.45 m now stays at its high midday ~127 ppm level into the late afternoon and evening, and air-RH rises steeply during the moist evening. Ground frost appears here already at 2200 LTST, despite the wind, and rapidly depletes water vapor from the air (Fig. 6, top, pr = 0). Air-RH nevertheless keeps increasing, although at a reduced rate after 2200 LTST, and fog forms at 1.45 m now about half an hour before sunrise.

In both experiments the deposited frost and the condensed thin icefog sublimate back to vapor and mix to the air soon after sunrise. Hence air-vmr at 1.45 m jumps suddenly (from about 35 ppm at dawn to 130 and 160 ppm at 0900 LTST, respectively), then returning to ~127 ppm during the afternoon. With weaker Vg and pr = 0 fog appears earlier (at 0400 LTST for 2 m/s and 0200 LTST for 0.5 m/s). Frost always appears at around 2200 LTST although the maximum predicted frost depth (at around 0700 LTST) increases slightly, from 0.33 μm with Vg 10 m/s to 0.50 μm with Vg of 0.5 m/s.

The latent heat effects associated with these phase changes of water are included in the model but they are much too small to have any impact on the air or ground temperatures. Boundary layer ice clouds such as observed at Phoenix did not appear in any of the present model experiments.

These experiments seem to further confirm that adsorption prevents fog and especially frost to occur on the relatively warm and dry low latitudes of Mars, as long as there is some wind near the surface. Frost and fog have certainly been observed on the midlatitude VL2 (48°N) and polar Phoenix (68°N) lander sites, These have been simulated by the SCM (Savijärvi, 2018; Savijärvi and Määttänen, 2010).

6. The scalar surface fluxes and free convection

The expression for the surface turbulent heat flux H_o based on the Monin-Obukhov similarity theory was presented and calculated for the first 350 sols from the hourly MEDA observations of WS, ATS, TIRS and PS in Martínez et al. (2023). SCM applies the same expression for H_o but here with the stability functions Z and G (Section 2), which better allow for extreme stratifications. In windy (near-neutral) conditions they are practically the same as those used by Martínez et al. (2023). We assume in lack of observations (as did Martinez et al.) that the roughness height z_o for scalars is the same as that for momentum, 1 cm.

The diurnal H_o is shown in Fig. 7 (top) from SCM simulations with V_g of 10, 2 and 0,5 m/s. The surface heat flux is quite small and downward (< 0) during the night hours; only −0.5…-1 W/m^2 for V_g of 10 m/s and very nearly 0 for the weaker winds. It increases rapidly when the ground gets heated by sunshine and T_g becomes warmer than the air, facilitating convection. Wind helps to transfer heat from the warm ground to the air in wind-forced convection, so the highest midday value for H_o, about 14 W/m^2, is reached in the windy reference simulation. These hourly values are quite similar to the mean hourly values of H_o calculated using observed winds during the first 350 sols (Martínez et al., 2023, Fig. 8e).

Interestingly, H_o is slightly higher in midday in the nearly calm simulation (Vg 0.5 m/s) than in the weak-wind (Vg 2 m/s) simulation The Richardson number is in the surface layer $Ri = (g/T_a)(T_a\text{-}T_g)z_a/V_a^2$, where V_a and T_a are wind speed and air temperature at height z_a and g is gravity (3.72 m/s^2 for Mars). In convective conditions ($T_g > T_a$) -Ri hence increases rapidly with decreasing V_a, and so do the G-functions of f(Ri) (Table 1), as free convection ($V_a \rightarrow 0$) is approached. The midday heat flux appears therefore nearly wind-independent in the nearly calm conditions. The effect of the locally more or less random-like large-eddy gusts, common during convective conditions in Mars (Petrosyan et al., 2011), are however not taken into account in our simulations.

Besides the dominating IR absorption (mainly by air-CO_2) of the thermal radiation from the hot ground, also the surface heat flux

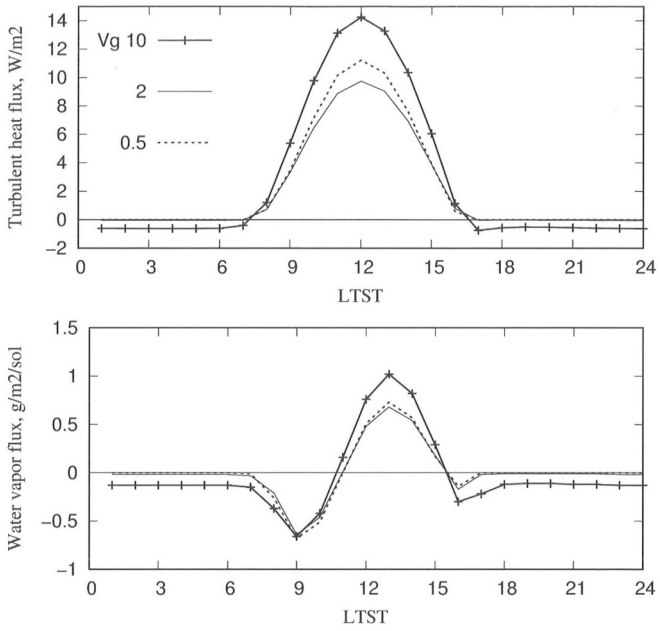

Fig. 7. Turbulent surface heat flux H_o (top), and water vapor flux out of regolith (bottom) in the three SCM simulations of Figs. 3–5 with V_g of 10 m/s (windy), 2 m/s (weak wind) and 0.5 m/s (nearly calm).

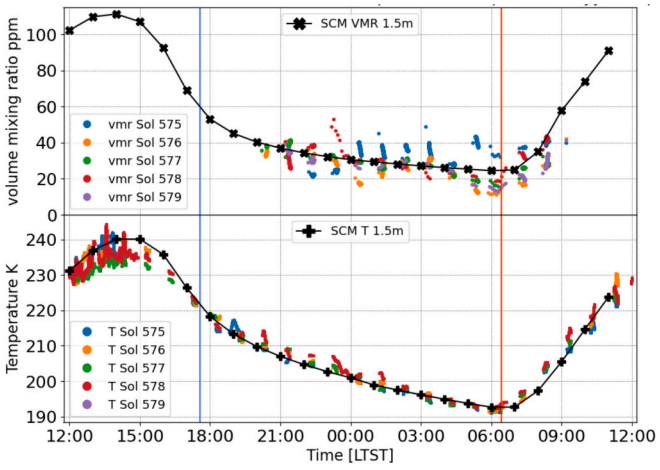

Fig. 8. MEDA water vapor volume mixing ratios (vmr) at 1.45 m height for sols 575–579 (τ ~ 1.6–1.76, top), and the respective ATS single-mast air temperatures at 1.45 m (bottom) in local true solar time (LTST). Curves are vmr and T at 1.45 m height from SCM simulations for τ = 1.6 and geostrophic wind speed of 10 m/s. Blue and red vertical lines indicate sunset and sunrise in LTST. (For interpretation of the references to colour in this figure legend, the reader is referred to the web version of this article.)

contributes a little to warm up the daytime near-surface air on Mars (Savijärv, 2012). This is here seen in Fig. 3: the afternoon air temperatures are higher in the windy simulation than in the other two simulations with weaker winds and hence slightly lower daytime H_o.

The respective modeled turbulent surface water vapor fluxes out of regolith are shown in Fig. 7 (bottom). The vapor flux is downward and small during the night hours. It is nearly zero during weak wind, when the vertical mixing of vapor by the shear-driven turbulence is almost nonexistent. However, after sunrise convection starts to mix water vapor strongly in the inversion of moisture, bringing down many more water molecules and thereby enhancing adsorption and the water intake to the regolith (as already noted by Zent et al., 1993). By about 0900 LTST the

shallow inversion is mixed away and the soil is warming up rapidly. Hence desorption takes over, leading to an upward water vapor flux, which peaks at around 1300 LTST, being, like H_o, nearly independent of wind speed in the weak-wind free convection conditions. Adsorption appears again when T_g cools rapidly in the late afternoon.

The sol-averaged water vapor flux is nearly zero. Hence pwc is approximately conserved from sol to sol, and about 0.1 g/m^2 of water (~1% of pwc) is here diurnally exchanged between the regolith and the air column in the windy simulation. This daily "breathing" of water through the surface of Mars is hence quite a reversible process from sol to sol.

7. The dusty experiment

The dusty airmass arrived to the site at around sol 572 and peaked on sols 576–578 (Ls 315°-316°) with observed τ being 1.58–1.76 (Fig. 1). In our dusty-case simulation Ls is set to 315.5° and τ conservatively to 1.6. All the other parameters are kept the same as in the windy reference simulation of Section 3. Because the rover did not move, the ground parameters stay the same, and we in fact hereby test, whether the moisture content in the arriving dusty air is the same as it was in the low-dust high-RH air mass it replaces at the site.

Fig. 8 displays vmr and air-T at 1.45 m from the dusty observations and from SCM. The afternoon air temperatures are now cooler and the dawn temperatures are higher than in the low-dust sols of Fig. 3. The model-T fits nicely within the nocturnal observations. The dustiest sol 577 (green, τ = 1.76) displays the lowest observed afternoon values of T, as can be expected. The model with the slightly lower τ of 1.6 produces a slight overestimate compared to that, again as expected.

The observation-based nocturnal values of vmr of Fig. 8 are around 20–40 ppm, as in Fig. 3, so the arriving dusty airmass appears to have about the same content of near-surface absolute moisture as the one it replaced. Sol 575 (blue dots) may have encountered weaker winds after midnight, as the vmr-values then jump from around 20 ppm to around 40 ppm. In contrast, the other sols may have been windy instead near the dawn, as their vmr-values then drop from about 30 ppm to below 20 ppm. This would be caused by enhanced adsorption due to the increased turbulence.

Fig. 9 shows the observed and modeled values of RH at 1.45 m and T_g, together with model-RH at the surface and model-T at 1.45 m. The superadiabatic T-gradient at daytime and the typical nocturnal inversion of 3–4 K between T_g and T at 1.45 m is nicely demonstrated in Fig. 9. Model-T_g (with TI of 300 SI units) matches here the observed T_g nearly perfectly (except again for a weak cold bias after sunrise), so the TIRS FoV represents here adequately the larger regolith-dominated region around the rover and the model's fast radiation algorithms appear to work well for the increased dust. The noon albedo from TIRS-FoV observations had increased here from 0.15 to 0.16 by sol 578, probably due to sedimented dust, whereas the FoV-based observed TI stayed at around 280 SI units.

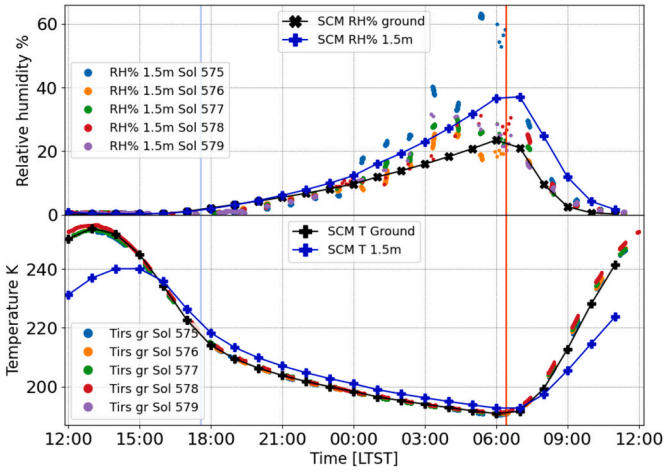

Fig. 9. As Fig. 8 but for MEDA HS-derived relative humidities and TIRS-observed ground temperatures, with SCM results. ATS-T and SCM-T at 1.45 m were compared in Fig. 8.

While the observation-based water vapor partial pressure p and vmr appear to be much the same in the dusty air mass as in the previous low-dust air mass, the observed dusty-air relative humidities RH = p/p_{sat}(T) are instead a lot lower, because the dust-enhanced high nocturnal air temperatures force p_{sat}(T) to be high. The SCM values of RH (blue line in Fig. 9) match the observation-derived low values of RH quite well, except near the dawn. The high observed near-dawn values of RH on sol 575 (blue dots in Fig. 9) might suggest weak wind, as did the blue high-vmr dots in Fig. 8. The other sols in Figs. 8–9 with their low near-dawn RH and vmr might indicate instead temporarily stronger near-dawn winds than what is typical for the season and site.

8. Concluding remarks

The diurnal martian water cycle was studied at a Jezero crater base delta front site during a cool midwinter period, using the M2020 mission observations and adsorptive column modeling. The Perseverance rover stayed parked on sols 566–591 just before the arrival of a dust event, and during the event. In the low-dust sols 566–571 (Ls 308°-312°, τ ~ 0.5) the HS-ATS derived air relative humidity at 1.45 m height (RH) was high, typically 40–90% near dawn, with occasional values >100%. With the typical nocturnal wind speed of 2 m/s at 1.45 m height (Vg being 10 m/s) and the typical column water content for the season and site (model-pwc of 9.7 μm), the model's diurnal air temperatures, RH and the water vapor volume mixing ratios (vmr) at 1.45 m were within the set of available observations during the period.

Unfortunately, wind observations were not available. When weaker winds were applied in the model, the nocturnal wind-driven turbulence, the induced water vapor flux toward the cold porous regolith, and the depleting adsorption of vapor onto the regolith grains all became weaker. Hence the near-surface air-vmr stayed high and model-RH increased rapidly with the decreasing temperatures. Temporarily weak winds might hence explain the high observed, even >100% values of RH and vmr during some of the nights. Such observed RH well above or below the average nocturnal trend might thus be a proxy for the current near-surface wind speed being below or above the typical near-surface wind speed of the hour.

In a nearly calm simulation thin radiation fog formed at 1.45 m at around 0300 local time, then grew upward to 40 m by sunrise and sublimated soon thereafter. Ground frost did appear at around 2200–2300 LT independently of wind speed, but only if adsorption or soil porosity was disabled in the simulation. Frost is hence most likely to appear first on rocks and exposed bedrock.

Fogs and especially frost are rare in the relatively dry and warm low latitudes of Mars, as the nocturnal adsorption to regolith acts as an effective cold trap of water vapor in the typically windy conditions. Radiation fogs might nevertheless exist during cold, moist and calm nights (as on the Earth), and be detectable e.g., in blurred camera pictures taken around and after dawn. The general circulation and mesoscale models of Mars do not usually include adsorption; hence they might tend to overpredict nocturnal frosts and fogs.

Interestingly, in the weak-wind experiments (simulating conditions of free convection), the modeled daytime turbulent surface fluxes of both heat and humidity tended to increase with decreasing ambient wind speed, when using the more recent stability functions, which approach the energetically correct limit of free convection.

The diurnal MEDA ground and air temperatures, RH and vmr were well simulated also during the dust peak period (sols 576–578, Ls 315°-316°, τ 1.6–1.8), when using the same ground parameters, wind (Vg of 10 m/s) and initial vertically constant (i.e., well-mixed) vmr as before

the dust event. Hence the arriving dusty and probably windy airmass appeared to have much the same near-surface absolute humidity (vmr) as the one it replaced. However, the observed and modeled relative humidities dropped dramatically, due to the dust-enhanced high nocturnal temperatures, through their strong impact on the saturation water vapor partial pressure.

Summarizing, the model experiments demonstrate the strong role of wind and dustiness in the martian surface layer.

CRediT authorship contribution statement

Hannu Savijärvi: Writing – original draft, Visualization, Validation, Supervision, Software, Methodology, Investigation, Formal analysis, Conceptualization. **Jouni Polkko:** Visualization, Validation, Software, Resources, Methodology, Investigation, Formal analysis, Data curation. **Maria Hieta:** Visualization, Validation, Resources, Investigation, Data curation. **German Martinez:** Writing – review & editing, Visualization, Validation, Resources, Methodology, Data curation. **Maria-Paz Zorzano:** Writing – original draft, Resources, Methodology, Data curation. **Leslie Tamppari:** Writing – review & editing, Validation, Methodology, Formal analysis, Data curation. **Joonas Leino:** Visualization, Validation, Software, Methodology, Formal analysis. **Mark Paton:** Visualization, Validation, Methodology, Formal analysis, Data curation. **Ari-Matti Harri:** Validation, Supervision, Resources, Project administration, Methodology, Funding acquisition, Formal analysis, Data curation.

Declaration of competing interest

The authors declare that they have no known competing financial interests or personal relationships that could have appeared to influence the work reported in this paper.

Data availability

Data will be made available on request.

Acknowledgements

The *Z*-Cam dust opacity values were kindly provided by Mark Lemmon. HS and AMH are grateful for the Academy of Finland grant #357577. GM wants to acknowledge JPL funding from USRA Contract Number 1638782. M.-P.Z was supported by grant PID2022-140180OB-C21 funded by MCIN/AEI/10.13039/501100011033/FEDER, UE. Part of this research was carried out at the Jet Propulsion Laboratory, California Institute of Technology, under a contract with the National Aeronautics and Space Administration (80NM0018D0004).

References

Garratt, J.R., 1992. The Atmospheric Boundary Layer. Cambridge Univ. Press, Cambridge.

Grachev, A.A., Fairall, C.W., Bradley, E.F., 2000. Convective profile constants revisited. Boundary-Layer Meteor. 94, 495–515.

Harri, A.-M., et al., 2024. Perseverance MEDA atmospheric pressure observations - initial results. J. Geophys. Res. Planets 129 e2023JE007880.

Hieta, M., et al., 2022. MEDA HS: relative humidity sensor for the Mars 2020 perseverance rover. Planet. Space Sci. 223, 105590 https://doi.org/10.1016/j.pss.2022.105590.210.

Jakosky, B.M., Zent, A.P., Zurek, R.W., 1997. The Mars water cycle: determining the role of exchange with the regolith. Icarus 130, 87–95.

Martínez, G., et al., 2023. Surface energy budget, albedo, and thermal inertia at Jezero crater, Mars, as observed from the Mars 2020 MEDA instrument, 2023. J. Geophys. Res. Planets 128 (2) e2022JE007537.

Munguira, A., et al., 2023. Near surface atmospheric temperatures at Jezero from Mars 2020 MEDA measurements. J. Geophys. Res. Planets 128 (3) e2022JE007559.

Newman, C.E., et al., 2022. The dynamic atmospheric and aeolian environment of Jezero crater, Mars. Sci. Adv. 8 (21), eabn3783.

Petrosyan, A., et al., 2011. The Martian atmospheric boundary layer. Rev. Geophys. 49, RG3005 https://doi.org/10.1029/2010RG000351.

Pla-García, J., et al., 2020. Meteorological predictions for Mars 2020 perseverance rover landing site at Jezero crater. Space Sci. Rev. 216 (8), 148.

Pla-García, J., et al., 2023. Nocturnal turbulence at Jezero crater as determined from MEDA measurements and modeling. J. Geophys. Res. Planets 128 (8) e2022JE007607.

Polkko, J., et al., 2023. Initial results of the relative humidity observations by MEDA instrument onboard the Mars 2020 Perseverance Rover. Journal of Geophysical Research: Planets 128, e2022JE007447. https://doi.org/10.1029/2022JE007447.

Rodriguez-Manfredi, J.A., et al., 2021. The Mars environmental dynamics analyzer, MEDA. A suite of environmental sensors for the Mars 2020 mission. Space Sci. Rev. 217, 48. https://doi.org/10.1007/s11214-021-00816-9.

Sánchez-Lavega, A., et al., 2023. Mars 2020 perseverance rover studies of the Martian atmosphere over Jezero from pressure measurements. J. Geophys. Res. Planets 128 (1) e2022JE007480.

Savijärv, H., 2012. Mechanisms of the diurnal cycle in the atmospheric boundary layer of Mars. Quart. J. Roy. Meteor. Soc. 138, 552–560. https://doi.org/10.1002/qj.930.

Savijärvi, H., 2018. New column simulations for the Viking landers: winds, fog, frost, adsorption? Icarus 310, 48–53. https://doi.org/10.1016/j.icarus.2017.11.007.

Savijärvi, H., Harri, A.-M., 2021. Water vapor adsorption on Mars. Icarus 357, 114270.

Savijärvi, H., Määttänen, A., 2010. Boundary-layer simulations for the Mars Phoenix lander site. Quart. J. Roy. Meteor. Soc. 136, 1497–1505. https://doi.org/10.1002/qj.650.

Savijärvi, H., Harri, A.-M., Kemppinen, O., 2016. The diurnal water cycle at curiosity: role of exchange with the regolith. Icarus 265, 63–69. https://doi.org/10.1016/j.icarus.2015.10.008.

Savijärvi, H., et al., 2020. Humidity observations and column simulations for a warm period at the Mars Phoenix lander site: constraining the adsorptive properties of regolith. Icarus 343, 113688.

Savijärvi, H., et al., 2022. Surface energy budget at curiosity through observations and column modeling. Icarus 376, 114900. https://doi.org/10.1016/j.icarus.2022.114900.

Savijärvi, H., Martinez, G.M., Harri, A., 2023. Surface energy fluxes and temperatures at Jezero crater, Mars. J. Geophys. Res. Planets 128. https://doi.org/10.1029/2022JE007438 e2022JE007438.

Viúdez-Moreiras, D., et al., 2022. Winds at the Mars 2020 landing site: 1. Near-surface wind patterns at Jezero crater. J. Geophys. Res. Planets 127 (12) e2022JE007522.

Zent, A.P., Haberle, R.M., Houben, H.C., Jakosky, B.M., 1993. A coupled subsurface-boundary layer model of water on Mars. J. Geophys. Res. 98 (E2), 3319–3337.

Zilitinkevich, S., Perov, V.L., King, J.C., 2002. Near-surface turbulent fluxes in stable stratification: calculation techniques for use in general-circulation models. Q. J. R. Meteorol.Soc 128, 1571–1587.

Zorzano, M.P., et al., 2024. Present-day thermal and water activity environment of the Mars sample return collection. Sci. Rep. 14, 7175. https://doi.org/10.1038/s41598-024-57458-4.